Dopaminergic Neurons Linking Threat Processing to Cardiac Modulation and Locomotor Responses

Masato Tsuji[1, *], Daisuke Jinkoma[1], Yuki Uemura[1], Ayako Ogasawara[1], and Kazuo Emoto[1, 2, *]

[1]Department of Biological Sciences, Graduate School of Science

[2]International Research Center for Neurointelligence (WPI-IRCN), The University of Tokyo, 7-3-1 Hongo, Bunkyo-ku, Tokyo, 113-0033, Japan

[*]Correspondence: mtsuji@bs.s.u-tokyo.ac.jp; emoto@bs.s.u-tokyo.ac.jp

TEL: +81-3- 5841-4426 FAX: +81-3- 5841-4632

Key words: Heart, Threat, Dopamine, Interoception, Drosophila

ABSTRACT

Heartbeat and behavior are tightly coordinated during defensive states, yet the neuronal mechanisms linking threat processing to cardiac modulation—and the potential contribution of cardiac dynamics to behavioral output—remain poorly understood. Here we show in *Drosophila* that mechanical threat triggers locomotion together with cardiac deceleration. We identify two dopaminergic neurons, termed DA-WED neurons, that mediate this cardiac response: silencing these neurons markedly attenuates threat-induced cardiac deceleration, whereas optogenetic activation induces cardiac deceleration in the absence of threat. Calcium imaging further shows that DA-WED neurons are activated by mechanical threat. Linking cardiac dynamics to behavior, direct optogenetic manipulation of cardiomyocytes that quantitatively reproduces threat-evoked cardiac deceleration is accompanied by increased locomotion. Together, these results identify a dopaminergic descending pathway that links threat processing to cardiac modulation and suggest that cardiac dynamics may contribute to shaping defensive behavior.

INTRODUCTION

Heartbeat dynamics are tightly coordinated with behavioral state. Defensive states, for example, are accompanied by coordinated modulation of cardiac activity, including transient cardiac deceleration during threat detection and cardiac acceleration during active coping in mammals[1]. Such tight coordination between behavioral state and cardiac dynamics is likely advantageous for survival: cardiac deceleration may minimize the brain-wide representations of the heartbeat[2–5] to sharpen sensory processing[16], whereas cardiac acceleration boosts the delivery of metabolic resources to muscles[7]. Although much of the existing work on heart–behavior coupling has focused on mammals, comparable threat-associated cardiac modulation has also been reported in invertebrates. In decapod crustaceans, for instance, sensory stimuli elicit time-locked heart rate changes that parallel defensive behaviors, suggesting that coordinated heart–behavior responses are evolutionarily widespread[8,9]. Despite this well-documented coupling, the circuit mechanisms linking threat processing in the brain to cardiac modulation—and whether cardiac dynamics contribute to behavioral output—remain incompletely understood.

In mammals, heartbeat is governed by sympathetic and parasympathetic branches of the autonomic nervous system (ANS) that innervate the heart[7,10–17]. Sympathetic output that accelerates the heartbeat arises from brainstem and hypothalamic circuits and projects through spinal intermediates to the heart[7]. On the other hand, the parasympathetic nervous system, which decelerates the heartbeat[7,18], originates from the dorsal motor nucleus of the vagus nerve and nucleus ambiguus, and projects directly to the heart[18,19]. These autonomic pathways are engaged in threatened animals by the so-

called fear circuitry in the brain[20–22] to shape cardiac responses, typically producing cardiac deceleration followed by acceleration[1,23–28]. Circuit-wise, the periaqueductal gray (PAG) is considered the output hub of the fear circuitry and modulates the heartbeat through the hypothalamus, midbrain, pons, and medulla oblongata[29]. In addition, hypothalamic nuclei such as the dorsomedial hypothalamus (DMH)[30] and the arcuate nucleus (ARC), as well as the anterior cingulate cortex (ACC)[31], also modulate the heartbeat upon threats[32–38].

In parallel, ascending feedback from the heart to the brain has attracted increasing attention. Such interoceptive signaling[39] is conveyed by sensory neurons innervating the heart and aortic arch[39], which project to NTS and onward to hypothalamic and cortical regions including paraventricular nucleus of the hypothalamus (PVN) [40], ACC, insular, and prefrontal cortex[40]. These pathways have been implicated in learned fear[41], anxiety-like behavior[42] or sleep[43]. Together, these findings suggest that bidirectional communication between brain and heart may shape physiological and behavioral responses during defensive states. However, how central circuits orchestrate threat-associated cardiac modulation, and whether cardiac dynamics influence defensive behavior, remain unresolved.

The fruit fly *Drosophila melanogaster* provides a genetically tractable system to dissect brain–body interactions. The *Drosophila* heart, an evolutionarily conserved organ[44–47], consists of two rows of cardiomyocytes forming a tubular structure that runs through the midline of the abdomen[48,49]. Like mammalian heart, *Drosophila* heart receives rich neuronal projections throughout[50,51]. Recent work has shown that visual

78 threat induces cardiac deceleration in *Drosophila*[52], suggesting the existence of the
79 neuronal mechanism in the brain that modulates the heart. However, the neuronal
80 substrate of such a mechanism, and the behavioral consequences of cardiac modulation
81 during threat, remain largely unknown.

82 We have recently reported that a train of air puffs elicit hyperactivity, avoidance of
83 puffs, and aversion from an otherwise neutral visual object, suggesting that air puffs
84 serve as mechanical threat[53]. Building on this work, we established an experimental
85 paradigm to assess how mechanical threat modulates heartbeat and behavior. Using this
86 system, we identify two pairs of dopaminergic neurons in the brain, termed DA-WED
87 neurons, that are responsible for threat-induced cardiac deceleration. We further
88 examine how cardiac deceleration relates to threat-induced locomotion. Together, our
89 findings identify a pair of dopaminergic neurons that link threat processing in the brain
90 to cardiac modulation and suggest that cardiac dynamics may contribute to shaping
91 defensive behavior.

RESULTS

I. Air puffs induce cardiac deceleration and locomotion

We have previously reported that a train of air puffs serve as mechanical threats, eliciting a host of fear-like behaviors such as hyperactivity, avoidance of puffs, and aversion from an otherwise neutral visual object[53]. This motivated us to test how the air puff might influence heartbeat, and its relation to behavior. For this purpose, we developed a paradigm to monitor heartbeat and behavior simultaneously (Fig. 1a). Our paradigm images the heart chamber closest to the thorax, called conical chamber, which is visualized through the dorsal cuticle by cuticle-penetrating infare-red light (Fig. 1a, "CAM1"). Simultaneously, the fly's behavior is recorded from the side of the fly (Fig. 1a, "CAM2"). We further developed a set of software to automatically detect heartbeat and behavior (Supplementary Movie 1). Our heartbeat detection software takes two consecutive frames and calculates for each pixel the optical flow, which are used to quantify the overall relaxation (diastole) or shrinkage (systole) of the heart (Supplementary Fig. 1a-c). Based on such quantification, our software detects the timings at which the heart was shrunk most (systole peak), which were counted to obtain the heart rate (HR). Our analysis pipeline for behavior detection first tracks the coordinate of body parts (joints of each leg, eye, neck, haltere, rostral tip of the abdomen, all on the right side of the fly), utilizing SLEAP software[54]. The tracked coordinates are then fed into our custom support vector machine-based program to detect locomotion. Our analysis pipeline allowed us to visualize the HR and locomotion over time in a synchronized fashion.

114 Using our paradigm, we tested how the air puff might influence the HR and
115 locomotion. Specifically, we applied for each fly a 0.5 s air puff (either 20 mL/min, 50
116 mL/min, 200 mL/min). We repeated 10 trials for each fly with an inter-puff interval of
117 90s (Fig. 1b). The results of 10 trials were averaged, as we did not observe noticeable
118 trial effects (Supplementary Fig. 2a, c). We found that the air puff transiently decreased
119 the HR (Fig. 1c-e; Supplementary Fig. 2a, b; Supplementary Movie 1). Similar
120 tendency was observed but was statistically insignificant for the strongest puff (200
121 mL/min), which is likely due to the following cardiac acceleration (Fig. 1d, e). Surgical
122 removal of body parts and silencing experiments of external sensilla or chordotonal
123 organ[55,56] suggest that hair plate neurons and chordotonal organs are at least partially
124 indispensable for puff-induced cardiac deceleration (Supplementary Fig. 3). We also
125 found that the air puff persistently increased the fraction of time walking, in line with
126 previous reports (Fig. 1f, g; Supplementary Fig. 2c, d)[53,57]. Thus, our data revealed that
127 the air puff induces cardiac deceleration and locomotion. Notably, in our paradigm the
128 air puff robustly induces locomotion and does not elicit sustained freezing, indicating
129 that the observed cardiac deceleration cannot be attributed to freezing-associated
130 bradycardia described in visually induced threat paradigms in flies[52] or in other contexts
131 in rodents[1]. This prompted us to next identify neurons responsible for cardiac
132 deceleration.

133

134 **II. Dopaminergic system is responsible for puff-induced cardiac deceleration**

135 To aid in identifying neurons responsible for cardiac deceleration, we developed yet
136 another paradigm to quantify the HR with higher throughput. In this paradigm, we

137 drove the expression of GFP in the cardiomyocytes using the enhancer of the Hand
138 gene[45], to aid in heartbeat imaging (Fig. 2a, b). GFP signals in pericardiocytes (also
139 known as nephrocytes) are likely due to their function to incorporate any molecules in
140 the hemolymph[58]. The fly's ventral side of the thorax and abdomen were glued to a
141 slide glass, and the GFP signals in the conical chamber were acquired through the intact
142 dorsal cuticle by confocal microscopy (Fig. 2a, b). The air puffs of 20 mL/min were
143 applied frontally to the fly's head through a glass pipette (Fig. 2a). Heartbeat was
144 detected using our custom software (Supplementary Fig. 4a-c). A single trial consisted
145 of 60 s of interval, 10 s of air puffs, and 60 s of recording, which was repeated twice for
146 each fly with 90s interval (Fig. 2c). This experiment revealed that air puffs induce
147 cardiac deceleration by roughly 10% (Fig. 2d-f; Supplementary Movie 2), consistent
148 with our earlier finding (Fig. 1). Similar results were obtained when the air puff was
149 applied for 1s (Supplementary Fig. 4d, e), 20s (Supplementary Fig. 4f, g), and in both
150 sexes (Supplementary Fig. 4h, i).

151 Monoaminergic systems have repeatedly been implicated in HR regulation across
152 species, including Drosophila[59–68]. We thus wondered whether monoaminergic systems
153 might be involved in puff-induced cardiac deceleration. When we silenced with TNT
154 the neurons expressing either serotonin, octopamine (insect equivalent of
155 norepinephrine), and dopamine, we found that silencing of octopaminergic or
156 dopaminergic neurons significantly suppressed puff-induced cardiac deceleration (Fig.
157 2g, h; Supplementary Fig. 5a, b). Note, however, that when we expressed in
158 serotonergic neurons the inward-rectifying potassium channel Kir2.1, it did decrease the
159 puff-induced cardiac deceleration (Supplementary Fig. 5c, d), suggesting that

160 serotonergic neurons may also be indispensable for puff-induced cardiac deceleration.
161 In line with this, a *loss-of-function* mutation of a serotonin synthetic enzyme *TrH* also
162 showed decrease in the puff-induced cardiac deceleration (Supplementary Fig. 5e-g).

163 To further probe the roles of monoaminergic neurons, we next tested whether
164 thermogenetic activation of these neurons can induce cardiac deceleration without air
165 puffs. To this end, we expressed a heat-gated cation channel dTrpA1 in monoaminergic
166 neurons, and shifted the temperature from 21°C to 28°C while monitoring the HR (Fig.
167 2i). This revealed that, while the HR of cold-blooded Drosophila increased as a function
168 the temperature even in the driver-less control (Fig. 2j, black), such cardiac acceleration
169 was suppressed by activation of dopaminergic neurons (Fig. 2j, blue) but not by
170 octopaminergic neurons (Fig. 2j, gray). On the other hand, activation of serotonergic
171 neurons exaggerated the heat-induced cardiac acceleration (Fig. 2j, red). The average
172 HR during 28°C period indeed revealed that the activation of dopaminergic neurons
173 significantly decreased the HR compared to the driver-less control, while the activation
174 of serotonergic neurons significantly increased the HR (Fig. 2k). Dopaminergic neurons
175 were the only monoaminergic population whose silencing and activation consistently
176 implicated them in driving cardiac deceleration (Fig. 2g-k). The role of dopaminergic
177 neurons is further reinforced by loss-of-function experiments of dopamine receptors,
178 which revealed that mutations of *Dop1R2* or *Dop2R* significantly decrease the puff-
179 induced cardiac deceleration (Fig. 2l, m; Supplementary Fig. 5h, i). A mutation of
180 *DopEcR* also showed a tendency to decrease the puff-induced cardiac deceleration
181 albeit not quite reaching the statistical significance (Fig. 2l, m; Supplementary Fig. 5h,
182 i). Together, our data demonstrates that dopamine system is responsible for puff-
183 induced cardiac deceleration.

184

185 **III. Two pairs of dopaminergic neurons in the brain, DA-WED neurons, are**
186 **indispensable for cardiac deceleration**

187 There are approximately 130 dopaminergic neurons scattered throughout the Drosophila
188 brain[69,70]. To identify the subpopulation of dopaminergic neurons responsible for puff-
189 induced cardiac deceleration, we turned to a host of dopamine-related GAL4 driver
190 lines[69] (Fig. 3a). Each of these drivers carries different bits of enhancers of dopamine-
191 related genes, and presumably for this reason these drivers are known to label partially
192 overlapping but distinct subpopulations of dopaminergic neurons[69]. When we drove the
193 expression of TNT by these drivers, we found that neuronal silencing by 4 out of 10
194 drivers decreased puff-induced cardiac deceleration (R76F01-, R76F02-, R76F05-,
195 R60F07-GAL4; Fig. 3b, blue plots) without significantly influencing the baseline HR
196 (Supplementary Fig. 6a), suggesting that these drivers label the subset of dopaminergic
197 neurons indispensable for puff-induced cardiac deceleration. Identification of these "hit"
198 drivers allowed us to next employ a split-GAL4 approach to further narrow down the
199 indispensable neurons (Fig. 3c). In the split-GAL4 method, the whole GAL4 protein is
200 split into the DNA-binding domain ("DBD") and the activation domain ("AD"), each
201 fused with a leucine-zipper domain[71]. When these "hemi-drivers" collide, they bind to
202 each other through their respective leucine zipper, re-constituting the functional GAL4.
203 Thus, by placing each of these hemi-drivers under different enhancers, one can achieve
204 the expression of functional GAL4 only in cells in which both enhancers are active (Fig.
205 3c). When we tested all split combinations of the 4 "hit" enhancers, we found that only
206 one combination, namely R76F05-DBD and R60F07-AD, significantly decreased the

207 puff-induced cardiac deceleration (Fig. 3d), without significantly influencing the
208 baseline HR (Supplementary Fig. 6b). Our immunohistochemical analysis revealed that,
209 as reported by a previous report[69], the split combination of R76F05-DBD and R60F07-
210 AD labeled two different subpopulations of dopaminergic neurons: one subpopulation
211 from the PPL1 cluster named PPL1-SMPγ, and another subpopulation from the PPM2
212 cluster named DA-WED (Fig. 3e), with additional one or two neurons occasionally
213 labeled in some brains. We further sought to identify which of these two subpopulations
214 is indispensable for puff-induced cardiac deceleration. Taking advantage of the
215 recently-developed analysis pipeline that identify a list of candidate GAL4 drivers that
216 may label any neuron of interest[72,73], we obtained a list of candidate PPL1-SMPγ and
217 DA-WED drivers. By testing several split combinations of enhancers used in these
218 drivers, we could identify the split combinations that label one but not the other (Fig.
219 3f). We note that each of these combinations labels additional neurons, in either
220 subesophageal zone (Fig. 3f, left) or optic lobes (Fig. 3f, right). Using these split
221 drivers, we silenced either PPL1-SMPγ or DA-WED with TNT, and found that
222 silencing of DA-WED significantly decreased puff-induced cardiac deceleration (Fig.
223 3g; Supplementary Fig. 6c). Together, our data suggests that DA-WED neurons are
224 indispensable for puff-induced cardiac deceleration.

225

226 **IV. DA-WED neurons are responsible for puff-induced cardiac deceleration**

227 While our data so far suggests the role of DA-WED neurons in cardiac deceleration, the
228 split driver we used to label DA-WED also labeled neurons in the optic lobes (Fig. 3f;
229 right). We thus further improved the labeling specificity through intersection strategy.

230 In this strategy, the effector gene is expressed under the control of UAS sequence, but a
231 "stop" sequence is inserted in between UAS and GFP, blocking the function of GAL4.
232 Now, the expression of "molecular scissors" called flippase (FLP) is driven by a
233 Tyrosine hydroxylase (TH) promoter ("TH-FLP"), which excises out the stop sequence.
234 Hence, GAL4 can function only in cells in which TH promoter is active. This strategy,
235 combined with our split GAL4 combination, indeed achieved near-perfect specificity
236 for DA-WED neurons, apparently labeling no other cells throughout the body (Fig. 4a;
237 Supplementary Fig. 6d). When we silenced DA-WED neurons with Kir2.1, it decreased
238 puff-induced cardiac deceleration (Fig. 4b, c), without noticeably influencing the
239 baseline HR (Supplementary Fig. 6e).

240 We next tested if DA-WED neurons function through dopamine. Our dopamine
241 receptor mutant analysis (Fig. 2l, m) suggests that dopamine signaling through Dop1R2
242 and Dop2R is indispensable for cardiac deceleration. Consistent with this, we found that
243 RNAi of a dopamine synthesis enzyme ple in DA-WED neurons reduced puff-induced
244 cardiac deceleration (Supplementary Fig. 6f-h). It is thus plausible that DA released
245 from DA-WED neurons binds to Dop1R2 and/or Dop2R to drive cardiac deceleration.

246 DA-WED neurons have previously been reported to drive protein preference
247 behavior in protein-deprived flies[74,75]. Indeed, suppression of DA-WED neurons
248 decreased protein preference (Supplementary Fig. 7a-d)[74,75] in addition to cardiac
249 deceleration (Supplementary Fig. 7e, Fig.4b, c). This prompted us to ask whether these
250 neurons drive cardiac deceleration and protein preference through shared, or instead
251 distinct, mechanisms. Interestingly, *Dop2R* mutant flies failed to show cardiac
252 deceleration (Fig. 2l, m), but showed normal preference compared to the wildtype

253 (Supplementary Fig. 7f, g). Similarly, suppression of FB-LAL neurons, through which
254 DA-WED neurons drive protein preference[74,75], failed to influence cardiac deceleration
255 (Supplementary Fig. 7h, i). These results suggest that DA-WED neurons drive protein
256 preference through FB-LAL neurons, while driving cardiac deceleration through Dop2R
257 independent of FB-LAL. This hypothesis is further reinforced by our observations that
258 protein deprivation, which drives protein preference (Supplementary Fig. 7j), fails to
259 influence puff-induced cardiac deceleration (Supplementary Fig. 7k) nor the baseline
260 HR (Supplementary Fig. 7l). Together, our data suggests that DA-WED neurons drive
261 cardiac deceleration and protein preference through distinct mechanisms
262 (Supplementary Fig. 7m).

263 We next wondered how DA-WED neurons might respond to air puffs. To this end,
264 we expressed jGCaMP7s in DA-WED neurons, and imaged their calcium activities
265 while applying a train of air puffs (Fig. 4d). We found that the calcium level of DA-
266 WED neurons steadily increased as air puffs are applied (Fig. 4e, f; Supplementary Fig.
267 8a; Supplementary Movie 3). The increased jGCaMP7s signals returned to the baseline
268 in less than 5 s when puffs ceased (Fig. 4f). Given the slow kinetics of jGCaMP7s[76], the
269 increased activity of DA-WED neurons likely returns to the baseline immediately when
270 the puffs cease. While there are two pairs of DA-WED neurons in the brain, one pair
271 being more medial than the other, we found no noticeable difference in medial vs lateral
272 DA-WED neurons' activities in response to puffs (Supplementary Fig. 8b-d). Our data
273 suggests that all four DA-WED neurons transiently get activated by air puffs.

274 To test if increased activities of DA-WED neurons can replace the air puff to
275 induce cardiac deceleration, we photoactivated DA-WED neurons without puff

application (Fig. 4h). For this, we expressed a light-gated cation channel CsChrimson in DA-WED neurons, and shined light on the fly's head to activate these neurons. We found that the photoactivation of DA-WED neurons could induce cardiac deceleration by ~10% in the retinal-fed test flies, but not in the retinal-unfed control flies (Fig. 4i, j; Supplementary Movie 3).

Together, our data establishes that DA-WED neurons are responsible for puff-induced cardiac deceleration (Fig. 4k).

V. Cardiac interoception possibly contributes to threat-induced locomotion

Cardiac interoception has recently been implicated in modulating behavioral responses [41–43]. We therefore asked whether cardiac deceleration is associated with changes in locomotion in *Drosophila*. To test this, we silenced DA-WED neurons using Kir2.1 to block puff-induced cardiac deceleration, and assessed locomotor output. We found that silencing DA-WED neurons markedly suppressed puff-induced locomotion compared to controls (Fig. 5a, b). Conversely, photoactivation of DA-WED neurons using CsChrimson promoted locomotion in the absence of puff (Fig. 5c, d). These findings suggest that DA-WED neurons coordinate cardiac deceleration with locomotor responses during threat.

An alternative interpretation is that DA-WED neurons function as general threat detectors that broadly regulate puff-evoked behaviors. If this were the case, manipulating these neurons should affect all of behavioral outputs induced by puff. In addition to promoting locomotion, air puff suppressed grooming (Supplementary Fig.

298 9a, b). However, silencing DA-WED neurons failed to disrupt puff-induced grooming
299 suppression (Supplementary Fig. 9c, d), despite markedly reducing cardiac deceleration
300 (Fig. 4b, c) and locomotion (Fig. 5a, b). Likewise, photoactivation of DA-WED neurons
301 failed to suppress grooming (Supplementary Fig. 9e, f), while robustly inducing cardiac
302 deceleration (Fig. 4b, c) and locomotion (Fig. 5c, d). Thus, manipulation of DA-WED
303 neurons does not reproduce the full behavioral repertoire triggered by puff. These
304 findings argue against the idea that DA-WED neurons function as general threat
305 detectors and instead support a more specific role in coordinating cardiac and locomotor
306 responses.

307 To directly test whether cardiac deceleration can influence locomotion, we
308 optogenetically mimicked puff-induced cardiac deceleration by expressing the light-
309 gated anion channel GtACR1 in cardiomyocytes using Hand-GAL4 (Fig. 5e). We
310 selected an anion channel to prolong diastole, unlike a previous report using a cation
311 channel[77], as puff-induced cardiac deceleration is characterized by elongated diastolic
312 intervals (Fig. 1c). Brief green light pulses (28 ms; Fig. 5f) transiently arrested the heart
313 in diastole (Fig. 5g; Supplementary Movie 5), reducing heart rate by ~10% (Fig. 5h, i),
314 comparable to puff- and DA-WED-induced deceleration (Fig. 1d, e; Fig. 4i, j). Notably,
315 optogenetic induction of cardiac deceleration in cardiomyocytes—independent of
316 central dopaminergic activation—was accompanied by increased locomotion (Fig. 5j,
317 k). In contrast, this manipulation failed to alter grooming behavior (Supplementary Fig.
318 9g-i). These observations are consistent with the possibility that cardiac deceleration
319 may influence locomotor responses during threat.

Together, these findings identify DA-WED neurons that drive cardiac deceleration during threat and suggest that the resulting cardiac state may influence locomotor responses (Fig. 5l).

Altogether, these results identify a group of dopaminergic neurons that mediate threat-induced cardiac deceleration and point to a potential role of cardiac dynamics in shaping locomotor responses during threat.

DISCUSSION

Here we demonstrate that mechanical threat engages dopaminergic neurons that induce rapid cardiac deceleration and is associated with increased locomotion. Air puff stimulation elicited both cardiac deceleration and locomotor activation (Fig. 1), and we identified two pairs of dopaminergic neurons, termed DA-WED neurons, as key mediators of the cardiac response (Fig. 4). Silencing these neurons attenuated threat-induced cardiac deceleration and locomotion, whereas optogenetic activation of DA-WED neurons elicited both responses in the absence of threat (Fig. 4, Fig. 5). Moreover, direct optogenetic cardiac deceleration was accompanied by increased locomotion (Fig. 5), suggesting that cardiac deceleration may influence behavioral responses. Together, these findings support a model in which descending dopaminergic control of cardiac activity contributes to the coordination of physiological and behavioral responses to threat, potentially via interoceptive feedback from the heart.

342 **Cardiac deceleration accompanies active defensive locomotion**

343 Our data show that air puff stimulation induces cardiac deceleration together with
344 increased locomotion (Fig. 1). Stronger puff results in more pronounced locomotion but
345 diminished cardiac deceleration (Fig. 1d-g), suggesting that cardiac deceleration is
346 likely not simply a byproduct of locomotion.

347 Although cardiac deceleration is often associated with freezing in mammals[1],
348 cardiac deceleration has also been observed during early threat detection and orienting
349 responses[78], suggesting that it reflects engagement of a defensive processing rather than
350 motor inhibition *per se*. Consistent with this view, dissociation between threat-evoked
351 cardiac modulation and freezing has been reported across taxa. In mammals, for
352 example, disruption of autonomic output can abolish cardiac deceleration without
353 eliminating freezing[79], suggesting that cardiac deceleration is not merely a secondary
354 consequence of freezing. Similarly, in decapod crustaceans and *Drosophila*, visual
355 stimuli elicit reproducible and time-locked changes in heart rate that accompany both
356 freezing and fleeing[8,9,80]. Our findings extend these observations by showing that
357 cardiac deceleration can accompany active fleeing behavior in response to mechanical
358 threat. Thus, cardiac deceleration is not restricted to passive defensive strategies but can
359 occur during active locomotor responses, supporting the idea that cardiac dynamics are
360 flexibly coupled to different components of the defensive repertoire.

361

362 **Dopaminergic neurons in the brain are responsible for puff-induced cardiac**
363 **deceleration**

364 The present study identifies two pairs of dopaminergic neurons in the brain, termed DA-
365 WED neurons, as key mediators of puff-induced cardiac deceleration. Silencing/
366 photoactivating DA-WED neurons disrupts/ mimics puff-induced cardiac deceleration,
367 respectively (Fig. 4b, c, h-j). Furthermore, DA-WED neurons exhibit calcium elevation
368 upon air puffs (Fig. 4d-g). Moreover, knockdown of the dopamine synthetic enzyme *ple*
369 in DA-WED neurons suppresses puff-induced cardiac deceleration (Supplementary Fig.
370 6f–h), suggesting that dopamine release from these neurons is required for cardiac
371 deceleration.

372 Circulatory dopamine has long been associated with cardiac acceleration across
373 species[81]. In *Drosophila*, pharmacological application of DA to the exposed heart
374 accelerates the heartbeat[60–63], seemingly at odds with our findings. However, the
375 responsible source of circulatory DA or DA receptor, as well as whether DA directly
376 acts on cardiomyocytes or instead through some yet unidentified cells, remain elusive.
377 In mammals, cardiomyocytes *per se* synthesize DA and express DA receptors, hinting
378 at autocrine mechanism[81]. Circulatory DA also increases the levels of epinephrine and
379 norepinephrine, complicating the interpretation of ”DA-induced” cardiac acceleration[82].
380 From our ple RNAi experiment (Supplementary Fig. 6f-h), DA released from DA-WED
381 neurons appears indispensable for puff-induced cardiac deceleration. Notably, neurites
382 of DA-WED neurons never exit the brain, suggesting that DA-WED neurons engage
383 circulation or yet unidentified neuronal circuitry to indirectly modulate the heartbeat.
384 Circulation is unlikely to mediate DA-WED neurons’ function, however, given that the

385 air puff and DA-WED activation both induce cardiac deceleration within a second (Fig.
386 1, Fig. 4). Interestingly, DA acting as a local neuromodulator to drive cardiac
387 deceleration has been documented in mammals by a few literatures, either in the ventral
388 tegmental area (VTA) or lateral habenula (LHb)[83,84]. Together, our findings and
389 previous literature suggest that dopamine may act not only as a circulating hormone that
390 accelerates heart rate, but as a centrally deployed neuromodulator capable of driving
391 cardiac deceleration during defensive states.

392

393 **DA-WED neurons coordinate cardiac and behavioral threat responses**

394 Across species, threatening stimulation elicits cardiac and behavioral responses in an
395 orchestrated fashion. Cardiac interoception is postulated to serve as key feedback to link
396 cardiac and behavioral responses[39]. Cardiac interoception is mediated by sensory
397 neurons innervating the heart and aortic arch[39], which convey information to ACC,
398 insular, and prefrontal cortex[40] through brain stem NTS and hypothalamic PVN[40]. These
399 ascending pathways have been proposed to modulate learned fear[41], anxiety-like
400 behavior[42] or sleep[43]. Although models propose that descending control of the heart and
401 ascending interoceptive feedback jointly shape defensive behavior, experimental
402 validation of this bidirectional framework within a single system has been limited.

403 Our results provide partial support for such a model. We show that (1) mechanical
404 threat induces cardiac deceleration and locomotion (Fig. 1), (2) DA-WED neurons in
405 the brain are responsible for threat-induced cardiac deceleration (Fig. 4), (3) optogenetic
406 cardiac deceleration is accompanied by increased locomotion (Fig. 5d-j). Our data

407 points to a scenario in which DA-WED neurons induce cardiac deceleration upon threat,
408 which may in turn influence threat-induced locomotion (Fig. 5k).

409 Notably, the behavioral consequences of cardiac deceleration appear to be selective
410 rather than global. Although air puff stimulation suppressed grooming, neither silencing
411 nor activation of DA-WED neurons significantly affected grooming responses
412 (Supplementary Fig. 9), despite robust effects on cardiac deceleration and locomotion
413 (Fig. 4, Fig. 5). Similarly, direct optogenetic induction of cardiac deceleration failed to
414 influence grooming behavior. These dissociations indicate that cardiac feedback does
415 not uniformly modulate defensive behaviors but preferentially facilitates locomotor
416 output. Such selectivity is consistent with the possibility that interoceptive signals from
417 the heart may bias specific behavioral strategies rather than simply increasing overall
418 arousal.

419 Our data suggest that descending dopaminergic control of cardiac function and
420 ascending cardiac feedback may form a functional loop that shapes adaptive defensive
421 behavior. Although the specific cardiac sensory pathways mediating feedback to the
422 brain remain to be identified in *Drosophila*, future work may determine whether flies
423 possess interoceptive circuits functionally analogous to vertebrate NTS–PVN pathways.
424 Establishing such circuitry would provide a powerful platform to dissect how central
425 commands and peripheral physiological states interact to coordinate survival behaviors.

426

427 **Limitations of this study**

428 While our data are consistent with a model in which DA-WED neurons couple
429 cardiac deceleration to locomotor responses during threat, several questions remain.

Although cardiac deceleration can promote locomotion, we have not directly tested whether it is required for DA-WED–evoked locomotion, leaving open the possibility of parallel downstream pathways. In addition, the sensory mechanisms that relay cardiac state to locomotor circuits in *Drosophila* remain unidentified. Finally, despite the rapid timescale and behavioral specificity of our manipulations, we cannot fully exclude indirect physiological contributions secondary to altered cardiac dynamics. Future dissection of descending and ascending circuits will clarify these mechanisms.

Overall, we identify a discrete population of dopaminergic neurons that drive rapid cardiac deceleration in response to mechanical threat. We further show that these neurons coordinate cardiac responses and are associated with behavioral components of the defensive response, potentially by engaging interoceptive feedback from the heart. Our findings establish *Drosophila* as a tractable model for dissecting how exteroceptive and interoceptive signals are integrated to couple organ physiology with adaptive behavior, opening new avenues for understanding the neural logic by which internal and external states are coordinated to promote survival.

446 **ONLINE METHODS**

447 **Fly stocks**

448 The following strains were obtained from Bloomington Stock Center (Indiana
449 University): TrH-GAL4 (#38388), Tdc2-GAL4 (#9313), TH-GAL4 (#8848), UAS-TNT
450 (#28838), UAS-Kir2.1::EGFP (#6596), UAS-CsChrimson::mVenus (#55135), UAS-
451 dTrpA1 (#26263), UAS-mCD8::GFP (#32186), UAS-RedStinger (#8547), UAS-IVS-
452 jGCaMP7s (#79032), UAS-GFP RNAi (#41560), UAS-Ple RNAi (#65875), VT046828-
453 AD (#73115), R12D12-DBD (#69213), R48A08-AD (#70707), VT008692-DBD
454 (#86909), empty-AD; empty-DBD (#79603), R70G12-GAL4 (#39552), R38B08-AD
455 (#71032), R81E10-DBD (#68529),VT043775-DBD (#73728), R74C07-GAL4
456 (#39847), Aes1N-GAL4 (#39847), iav-GAL4 (#52273), R48A07-GAL4 (#50340),
457 UAS-mCherry (#52267), Hand-GAL4 (#48396).

458 The following strains were obtained from Kyoto Drosophila Stock Center (Kyoto
459 Institute of Technology): Tes1N-GAL4 (#103660).

460 Hand-GFP was a gift from Dr. Zhe Han (The University of Maryland).

461 UAS-FRT-stop-FRT-Kir2.1, and UAS-FRT-stop-FRT-CsChrimson::mVenus were
462 gifts from Dr. Barry Dickson (The University of Queensland).

463 TH-C-GAL4, TH-D-GAL4, TH-F1-GAL4, Vmat-R76F01-GAL4, Vmat-R76F05-
464 GAL4, Ddc-R61H03-GAL4, Ddc-R60F07-GAL4, DAT-R55C10-GAL4, Vmat-
465 R76F01-AD, Vmat-R76F05-AD, Ddc-R60F07-AD, Vmat-R76F01-DBD, Vmat-
466 R76F05-DBD, Ddc-R60F07-DBD, TH-FLP, UAS-FsF-mCD8GFP were gifts from Dr.
467 Mark Wu (Johns Hopkins University).

468 *Dop1R1-attP*, *Dop1R2-attP*, *Dop2R-attP*, *DopEcR-attP, TrH-attP* were gifts from
469 Dr. Yi Rao (Peking University).

470 UAS-GtACR1::tdTomato (III) was gift from Dr. Tabata (The University of Tokyo).

471 Genotypes and sample sizes used in this study are summarized in Supplementary
472 Data 1.

473

474 **Fly husbandry**

475 Flies were maintained on conventional cornmeal-agar-molasses medium under a
476 9AM:9PM light/ dark cycle at 25 ˚C and 60 +/- 5 % humidity. Flies were collected 0–1
477 day post eclosion and housed in a group of 9-10 for 2-5 days before testing unless
478 otherwise stated. Male flies were used throughout except for Supplementary Fig. 4h, i,
479 in which both male and female were used. All experiments were carried out between 10
480 am and 8 pm at 25 +/- 0.8 C and 60 +/- 5 % humidity.

481

482 **Heartbeat and behavior recording**

483 Flies were tethered above an air-supported foam ball (8 mm diameter; Yuzawaya,
484 Japan) mounted in a custom sphere holder. Airflow was continuously monitored using a
485 digital flowmeter (MF-FP10N-H06-010, Horiba Estec Inc.) and maintained at 500 ± 10
486 mL/min. Behavioral imaging was performed from the right side under 850 nm infrared
487 illumination using a CMOS camera (GE60, Himawari; 640 × 480 pixels).
488 Simultaneously, cardiac activity was imaged from the dorsal side through the intact
489 cuticle under 850 nm illumination using a second CMOS camera (CS135MU, Thorlabs;

490 800 × 500 pixels). Behavioral and cardiac imaging streams were externally triggered
491 and synchronized at 70 Hz using an Arduino Uno board.

492 Immediately prior to the experiment, flies were briefly (< 1 min) cold-anesthetized,
493 and the dorsal thorax and abdomen were glued to a coverslip using UV-curable
494 adhesive (Bondic BD-SKCJ) polymerized with 405 nm UV light (OSV5XME1C1E,
495 Akizuki Electronics Inc.). The coverslip was positioned above the air-supported ball,
496 allowing the fly to freely walk on the ball. Each recording session, except for DA-WED
497 optogenetic activation experiment, consisted of a 20 min acclimation period followed
498 by puff-response testing (950 s). During puff-response testing, a 500 ms air puff was
499 delivered once every 90 s for a total of 10 puffs. Recording continued for 30 s after the
500 final puff. DA-WED optogenetic activation experiment consisted of a 20 min
501 acclimation period followed by photoactivation-response testing (950 s), in which a 1 s
502 617nm light was delivered once every 90 s for a total of two (See "Optogenetic
503 activation of DA-WED neurons" below), to avoid potential desensitization of
504 CsChrimson.

505

506 **Heartbeat (without behavior) recording**

507 Cardiomyocytes expressing GFP were imaged dorsally through the intact cuticle.
508 Images (104 × 50 pixels) were acquired at 24 Hz using a Leica SP8 confocal
509 microscope equipped with a 10× objective lens (NA 0.4).

510 Immediately before recording, flies were briefly (< 1 min) cold-anesthetized, and
511 the ventral thorax and abdomen were glued to a glass slide using UV-curable adhesive
512 (Bondic BD-SKCJ) polymerized with 405 nm UV light (OSV5XME1C1E, Akizuki

513 Electronics Inc.). The slide was positioned beneath the objective lens for imaging. Each
514 recording session consisted of a 10 min acclimation period followed by puff-response
515 testing (350 s total). A single puff-response test consisted of 1 min baseline recording,
516 followed by a train of 10 air puffs delivered at 1 Hz (10 s total), and a subsequent 1 min
517 post-stimulation recording. For each fly, the puff-response test was repeated twice with
518 a 90 s inter-trial interval.

519

520 **Automatic heartbeat detection**

521 To automatically detect individual heartbeats, we developed custom software tools. For
522 infrared (IR)–based heart imaging obtained during simultaneous recordings of cardiac
523 activity and behavior, the detection pipeline (Supplementary Fig. 1a) computed optical
524 flow for each pixel between consecutive video frames. These optical flow
525 measurements were used to quantify global cardiac relaxation (diastole) and contraction
526 (systole). Time points corresponding to maximal contraction were identified as systolic
527 peaks, and peak counts were used to compute heart rate (HR). The precision of the
528 automated detection was evaluated by comparing both absolute HR values and percent
529 changes in HR during air-puff stimulation relative to baseline with manual annotations.
530 These analyses demonstrated that the automated method detected both absolute HR and
531 stimulus-evoked HR changes with accuracy indistinguishable from manual scoring
532 (Supplementary Fig. 1b, c).

533 To detect heartbeats in confocal microscopy images of GFP-expressing
534 cardiomyocytes (recorded in the absence of behavioral measurements; Supplementary
535 Fig. 4a), each frame was subtracted from the subsequent frame to compute pixel-wise

536 differences between consecutive image pairs. This procedure generated positive and
537 negative pixel values in regions surrounding the cardiomyocytes during cardiac
538 contraction (systole) and relaxation (diastole). During systole, pixels within the heart
539 tube exhibited positive values corresponding to the current positions of cardiomyocytes,
540 whereas pixels outside the heart tube exhibited negative values corresponding to their
541 previous positions; the opposite pattern was observed during diastole. Systolic and
542 diastolic phases were distinguished by: (i) calculating the standard deviation of the
543 positions of positive-value pixels along the axis perpendicular to the heart tube (the y-
544 axis in Supplementary Fig. 4a), denoted SD(t); (ii) calculating the standard deviation of
545 the positions of negative-value pixels along the same axis, denoted SD(t–1); and (iii)
546 computing the difference SD(t) − SD(t–1). Negative values of SD(t) − SD(t–1)
547 indicated systole, whereas positive values indicated diastole (Supplementary Fig. 4a).
548 Time points corresponding to maximal contraction were identified as systolic peaks,
549 and peak counts were used to compute HR. The precision of this algorithm was
550 evaluated as described above. Although absolute HR values were slightly overestimated
551 (Supplementary Fig. 4b), stimulus-evoked changes in HR were captured with accuracy
552 indistinguishable from manual annotation (Supplementary Fig. 4c).

553 To obtain a continuous HR time course, peak counts were binned into 0.2 s
554 intervals, and the number of beats per bin was calculated for each fly and trial. For
555 visualization of HR dynamics relative to stimulus onset, HR traces were aligned to puff
556 onset (time 0) and averaged across repeated trials within each fly. In experiments with a
557 single air puff, puff-induced HR modulation was quantified by comparing the mean HR
558 during the 1 s following puff onset with the mean HR during the 10 s baseline period
559 preceding puff onset. Percent change was calculated as [(HR_post − HR_baseline) /

560 HR_baseline] × 100. In experiments involving 10 puffs delivered over a 10 s window,
561 HR modulation was quantified as the mean HR during the entire 10 s stimulation period
562 relative to the 10 s pre-stimulus baseline.

563

564 **Automatic behavioral identification**

565 To automatically identify behavior on a frame-by-frame basis, videos were analyzed
566 offline using a custom Python-based pipeline. Body-part coordinates—including the
567 joints of each leg, the eye, neck, haltere, and the rostral tip of the abdomen on the right
568 side of the fly—were tracked using SLEAP software[54]. The tracked coordinates were
569 subsequently transformed to normalize body length and orientation across individuals.
570 Using these standardized coordinates, the speed of each body part was calculated for
571 each pair of consecutive frames. Both the standardized coordinates and corresponding
572 speed measurements were then provided as inputs to a custom support vector machine
573 (SVM)–based classifier, which labeled each frame as "groom," "walk," or "halt." The
574 SVM was trained using the standardized body-part coordinates and speed features as
575 predictors, with manually annotated behavioral labels serving as the dependent
576 variables. For each fly and each time point relative to puff onset, we calculated the
577 fraction of frames classified as walking or grooming across 10 repeated trials. For
578 visualization of behavioral dynamics, these fraction time courses were aligned to puff
579 onset (time 0) and averaged across trials within each fly. Puff-induced changes in
580 walking and grooming were quantified by comparing the mean fraction during the 10 s
581 and 3 s, respectively, following puff onset with the mean fraction during the 10 s

582 baseline period preceding puff onset. Percent change was calculated as [(fraction_post −
583 fraction_baseline) / fraction_baseline] × 100.

584

585 **Mechanical stimulation**

586 Mechanical stimulation was delivered through a glass pipette (tip diameter of ~2 mm),
587 placed ~2mm in front of the fly, connected with air hose to a compressor (EARTH
588 MAN, Takagi, Japan) via a solenoid valve (EXA-C6-02C-4, CKD). The solenoid valve
589 was controlled by an Arduino Uno board, which in turn received connection from a
590 desktop computer running the python program which orchestrated the video recordings
591 and puff application. The mechanical stimulation was generated by alternating the
592 solenoid valve between 500 ms-open and 500 ms-closed states (1 Hz). The mechanical
593 stimulation lasted for either 1s, 10s, or 20s, as specified in each figure. The air flow was
594 monitored with a digital flowmeter (MF-FP10N-H06-010, Horiba estec. Inc) and was
595 adjusted to either 20 mL, 50 mL, or 200 mL/min, as specified in each figure.

596

597 **Optogenetic activation of DA-WED neurons**

598 Flies expressing CsChrimson, a red-shifted channelrhodopsin variant, in DA-WED
599 neurons were raised on food containing 500 μM all-trans retinal for 2 - 3 days, in the
600 dark, prior to testing. Photoactivation was performed by delivering a 1s LED light pulse
601 (617nm, Thorlabs) to the fly's head. The output for LED was measured with a power
602 meter (S120C and PM120D, Thorlabs) at a position corresponding to the fly's head, and
603 was adjusted to 1 $\mu W/mm^2$. Light stimuli were triggered by python through an Arduino
604 board connected to the LED driver.

605

606 **Optogenetic cardiac deceleration**

607 Flies expressing GtACR1, a light-gated anion channel, in cardiomyocytes were raised
608 on food containing 500 μM all-trans retinal for 2 - 3 days, in the dark, prior to testing.
609 Photoactivation was performed by delivering a 28ms-long LED light pulse (530nm,
610 Thorlabs) to the fly's heart through the objective lens. The light intensity was adjusted,
611 for each fly prior to the recording, to the minimum intensity required for a light pulse of
612 roughly 2s to briefly stop the heartbeat. After the recording, the output for LED was
613 measured with a power meter (S120C and PM120D, Thorlabs) at a position
614 corresponding to the fly's heart, and ranged from 9.88 – 21.8μW/mm^2. Light stimuli
615 were triggered by python through an Arduino board connected to the LED driver.

616

617 **Immunohistochemistry**

618 The following antibodies were used: mouse nc82 (1:10 Developmental Studies
619 Hybridoma Bank), goat anti-mouse Alexa 633 (1:100, Molecular Probe #A21050).
620 Whole brain immunohistochemistry was performed as described previously[85,86]. Briefly,
621 brains were dissected out in 0.3 % PBST, and were fixed in 2 % paraformaldehyde/
622 PBS for 90 min at room temperature. Brains were then washed in 0.3 % PBST, for > 3
623 h, and were blocked in 10 % normal goat serum/ 0.3 % PBST for 30 min. Brains were
624 incubated in the primary antibodies in 10% normal goat serum/ 0.3% PBST at 4 ˚C for 2
625 days. Brains were then washed in 0.3 % PBST for > 5 h, and were blocked in 10 %
626 normal goat serum/ 0.3 % PBST for 30 min. Brains were then incubated in the
627 secondary antibodies in 10 % normal goat serum/ 0.3 % PBST at 4°C for 2 days.

628 Afterward, brains were washed in 0.3 % PBST for > 5 h, and incubated in 50 %
629 glycerol/ 0.3 % PBST for 2 h at 4 ˚C. Lastly, brains were mounted on slide glass in
630 Vectashield (Vector Laboratories). Images were taken with Leica TCS SP8 confocal
631 microscope, and processed in ImageJ (NIH) software.

632

633 **Calcium imaging**

634 Two-photon calcium imaging was conducted as described previously[53] with a few
635 modifications. Two-photon microscopy (Bergamo II, Thorlabs) with a 16x objective
636 lens (16x CFI LWP Plan Flour Objective, Nikon) and with near-infrared excitation (930
637 nm, Mai Tai 2, SpectraPhysics. Inc., Mountain View, CA) was used. Cuticle of the top
638 of the flies' head and the fat and trachea beneath it were surgically removed. The
639 exposed brain was submerged in saline solution. The extracellular saline had the
640 following composition (in mM): 103 NaCl, 3 KCl, 5 HEPES, 10 trehalose, 10 glucose,
641 7 sucrose, 26 $NaHCO_3$, 1 NaH_2PO_4, 1.5 $CaCl_2$, 4 $MgCl_2$. We identified DA-WED
642 neurons using the baseline fluorescence of GCaMP. Images were acquired from 1 plane
643 at 152 frames per s (160 x 96 pixels, pixel size = 0.388 μm, dwell time = 0.246 μs).
644 During calcium imaging, a large fraction of the fly's body was glued to the holding
645 plate, and part of the fly's eye compounds was covered with the holder, and the fly was
646 hung in the air. Each fly underwent the sequence of stimuli per fly once or twice, to
647 scan DA-WED neurons on both hemispheres whenever possible. The time courses of
648 $\Delta F/F_0$ were calculated by, for each bin, taking the percent difference from F 10s prior to
649 the onset of the initial puff application (t = -10 through 0s in Fig. 4f).

650

651 **Surgery**

652 In search of sensory organs indispensable for air puffs to induce cardiac deceleration,
653 halteres, wings, legs, and a3 segments of the antennae were surgically removed using a
654 pair of forceps on ice just prior to testing. Flies that underwent cold anesthesia just prior
655 to testing served as controls.

656

657 **Feeding preference test**

658 Two days post eclosion male flies were protein deprived by maintaining on 200 mM
659 sucrose (vials with a kimwipe soaked with 2mL of sucrose solution) for 8 days
660 (kimwipe is exchanged every other day). Prep 7.5% yeast and 200mM sucrose in 0.9%
661 of agar, color-labeled with either blue (brilliant blue FCF) or red (sulforhodamine B)
662 tasteless food dyes. The two types of food mix, 1mL each, were then aliquoted into
663 35mm petri dish separated by a 5x5x35mm acrylic bar into two chambers. A group of
664 70 flies starved for 3 hours in an empty vial with a kimwipe soaked with 2 mL of water
665 were cold-anesthetized and transferred into petri dish at ZT2 and allowed to feed for 2
666 hours in the dark. The flies were then killed by transferring the dish to -30C, upside-
667 down, and scored by examining the color of their abdomen. Preference Index (PI) for
668 yeast was calculated as (# flies consuming yeast - # flies consuming sucrose) / (total #
669 flies that fed). Flies with insufficiently colored abdomen were discarded as poorly fed
670 flies.

671

672 **Data analyses**

673 Data analyses were performed using our custom-written R and python programs.

674

675 **Statistics**

676 We did not predetermine the sample sizes. The distribution of normality of each group
677 was assessed using Shapiro-Wilk normality test. Parametric tests (unequal variances *t*-
678 test known as Welch's *t*-test or Dunnett's test) were used only when distributions were
679 deemed normal; otherwise, non-parametric tests were used (Wilcoxon signed rank test,
680 Wilcoxon rank sum test, or Dunn's test). All statistical tests were two-sided. We
681 employed Bonferroni correction to correct for two tests, and correction implemented in
682 Dunnett's or Dunn's test for more than two tests. $p < 0.05$ after corrections for multiple
683 comparison was deemed statistically significant. Neither randomization nor blinding
684 was performed for the group allocation during experiments or data analysis. All box
685 plots are generated so that center line indicates median, box limits indicate upper and
686 lower quartiles, and whiskers indicate 1.5x interquartile range. All the statistical results
687 are summarized in Supplementary Data 2.

688

689 **DATA AVAILABILITY**

690 Source data for all main text and Supplementary Figures are available via request to the
691 corresponding author.

692

693 **CODE AVAILABILITY**

694 Source codes used in the current study are available at
695 https://github.com/mtsuji172/heart_behavior.

ACKNOWLEDGEMENTS

We thank T. Katsuki (ThorLabs) for technical support in setting up the hardware; members of the Emoto Lab for advice and support. This study was supported by JSPS (KAKENHI 24K18157), JST (ACT-X JPMJAX242D), Yamaguchi Educational and Scholarship Foundation to M.T., AMED-CREST (JP21gm310010), Takeda Science Foundation, Torray Foundation, Naito Foundation, and WPI-IRCN to K.E.

AUTHOR CONTRIBUTIONS

M.T. designed the experiments. M.T., J. D., Y. U., and A.O. performed the experiments. M.T. analyzed the data. M.T. and K.E. interpreted the results and wrote the paper.

COMPETING FINANCIAL INTERESTS

The authors declare no competing financial interests.

REFERENCES

1. Hagenaars, M. A., Oitzl, M. & Roelofs, K. Updating freeze: Aligning animal and human research. *Neuroscience and Biobehavioral Reviews* vol. 47 165–176 Preprint at https://doi.org/10.1016/j.neubiorev.2014.07.021 (2014).

2. Babo-Rebelo, M., Richter, C. G. & Tallon-Baudry, C. Neural Responses to Heartbeats in the Default Network Encode the Self in Spontaneous Thoughts. *Journal of Neuroscience* **36**, 7829–7840 (2016).

3. Jammal Salameh, L., Bitzenhofer, S. H., Hanganu-Opatz, I. L., Dutschmann, M. & Egger, V. Blood pressure pulsations modulate central neuronal activity via mechanosensitive ion channels. *Science* **383**, eadk8511 (2024).

4. Azzalini, D., Buot, A., Palminteri, S. & Tallon-Baudry, C. Responses to heartbeats in ventromedial prefrontal cortex contribute to subjective preference-based decisions. *The Journal of Neuroscience* **41**, JN-RM-1932-20 (2021).

5. Ran, C., Boettcher, J. C., Kaye, J. A., Gallori, C. E. & Liberles, S. D. A brainstem map for visceral sensations. **609**, (2022).

6. Lang, P. J., Davis, M. & Öhman, A. Fear and anxiety: Animal models and human cognitive psychophysiology. *J. Affect. Disord.* **61**, 137–159 (2000).

7. Gordan, R., Gwathmey, J. K. & Xie, L.-H. Autonomic and endocrine control of cardiovascular function. *World J. Cardiol.* **7**, 204 (2015).

8. Pérez-Schuster, V. *et al.* Threatening stimuli elicit a sequential cardiac pattern in arthropods. *iScience* **27**, 108672 (2024).

9. Burnovicz, A., Oliva, D. & Hermitte, G. The cardiac response of the crab Chasmagnathus granulatus as an index of sensory perception. *Journal of Experimental Biology* **212**, 313–324 (2009).

10. Koba, S. *et al.* A brainstem monosynaptic excitatory pathway that drives locomotor activities and sympathetic cardiovascular responses. https://doi.org/10.1038/s41467-022-32823-x (2022) doi:10.1038/s41467-022-32823-x.

11. Green, A. L. *et al.* Identifying cardiorespiratory neurocircuitry involved in central command during exercise in humans. *Journal of Physiology* **578**, 605–612 (2007).

12. Matsukawa, K. Central command: Control of cardiac sympathetic and vagal efferent nerve activity and the arterial baroreflex during spontaneous motor behaviour in animals. in *Experimental Physiology* vol. 97 20–28 (Blackwell Publishing Ltd, 2012).

13. Yoshimoto, A., Morikawa, S., Kato, E., Takeuchi, H. & Ikegaya, Y. Top-down brain circuits for operant bradycardia. *Science* **384**, 1361–1368 (2024).

14. Wink, J. *et al.* Human adult cardiac autonomic innervation: Controversies in anatomical knowledge and relevance for cardiac neuromodulation. *Autonomic Neuroscience: Basic and Clinical* vol. 227 Preprint at https://doi.org/10.1016/j.autneu.2020.102674 (2020).

15. White, D. W. & Raven, P. B. Autonomic neural control of heart rate during dynamic exercise: Revisited. *Journal of Physiology* vol. 592 2491–2500 Preprint at https://doi.org/10.1113/jphysiol.2014.271858 (2014).

16. Rajendran, P. S. *et al.* Identification of peripheral neural circuits that regulate heart rate using optogenetic and viral vector strategies. *Nat. Commun.* **10**, 1–13 (2019).

17. Silvani, A., Calandra-Buonaura, G., Dampney, R. A. L. & Cortelli, P. Brain-heart interactions: Physiology and clinical implications. *Philosophical Transactions of the Royal Society A: Mathematical, Physical and Engineering Sciences* vol. 374 Preprint at https://doi.org/10.1098/rsta.2015.0181 (2016).

18. Prescott, S. L. & Liberles, S. D. Internal senses of the vagus nerve. *Neuron* **110**, 579–599 (2022).

19. Veerakumar, A., Yung, A. R., Liu, Y. & Krasnow, M. A. Molecularly defined circuits for cardiovascular and cardiopulmonary control. *Nature 2022* 1–8 (2022) doi:10.1038/s41586-022-04760-8.

20. Silva, B. A., Gross, C. T., Gräff, J. & Gra, J. The neural circuits of innate fear : detection , integration , action , and memorization. *Learning and Memory* **23**, 544–555 (2016).

21. Headley, D. B., Kanta, V., Kyriazi, P. & Paré, D. Embracing Complexity in Defensive Networks. *Neuron* **103**, 189–201 (2019).

22. Gross, C. T. & Canteras, N. S. The many paths to fear. *Nat. Rev. Neurosci.* **13**, 651–658 (2012).

23. Kreibig, S. D. Autonomic nervous system activity in emotion: A review. *Biological Psychology* vol. 84 394–421 Preprint at https://doi.org/10.1016/j.biopsycho.2010.03.010 (2010).

24. Battaglia, S. & Thayer, J. F. Functional interplay between central and autonomic nervous systems in human fear conditioning. *Trends Neurosci.* **0**, (2022).

25. Casto, R., Nguyen, T. & Printz, M. P. Characterization of cardiovascular and behavioral responses to alerting stimuli in rats. *American Journal of Physiology-Regulatory, Integrative and Comparative Physiology* **256**, R1121–R1126 (1989).

26. Dielenberg, R. A., Carrive, P. & McGregor, I. S. The cardiovascular and behavioral response to cat odor in rats: unconditioned and conditioned effects. *Brain Res.* **897**, 228–237 (2001).

27. Signoret-Genest, J. *et al.* Integrated cardio-behavioral responses to threat define defensive states. *Nat. Neurosci.* **26**, (2023).

28. Hashemi, M. M. *et al.* Neural Dynamics of Shooting Decisions and the Switch from Freeze to Fight. *Sci. Rep.* **9**, (2019).

29. Farkas, E., Jansen, A. S. P. & Loewy, A. D. Periaqueductal gray matter input to cardiac-related sympathetic premotor neurons. *Brain Res.* **792**, 179–192 (1998).

30. Horiuchi, J., McDowall, L. M. & Dampney, R. A. L. DIFFERENTIAL CONTROL OF CARDIAC AND SYMPATHETIC VASOMOTOR ACTIVITY FROM THE DORSOMEDIAL HYPOTHALAMUS. *Clin. Exp. Pharmacol. Physiol.* **33**, 1265–1268 (2006).

31. Alexander, L. *et al.* Over-activation of primate subgenual cingulate cortex enhances the cardiovascular, behavioral and neural responses to threat. *Nat. Commun.* **11**, 1–14 (2020).

32. Koba, S., Inoue, R. & Watanabe, T. Role played by periaqueductal gray neurons in parasympathetically mediated fear bradycardia in conscious rats. *Physiol. Rep.* **4**, e12831 (2016).

33. Nakamura, K., Nakamura, Y. & Kataoka, N. A hypothalamomedullary network for physiological responses to environmental stresses. *Nature Reviews Neuroscience 2021 23:1* **23**, 35–52 (2021).

34. Hermans, E. J., Henckens, M. J. A. G., Roelofs, K. & Fernández, G. Fear bradycardia and activation of the human periaqueductal grey. *Neuroimage* **66**, 278–287 (2013).

35. Samuels, B. C., Zaretsky, D. V. & DiMicco, J. A. Tachycardia evoked by disinhibition of the dorsomedial hypothalamus in rats is mediated through medullary raphe. *Journal of Physiology* **538**, 941–946 (2002).

36. Rahmouni, K. Cardiovascular Regulation by the Arcuate Nucleus of the Hypothalamus. *Hypertension* **67**, 1064–1071 (2016).

37. Li, S. J. *et al.* Melanocortin antagonists define two distinct pathways of cardiovascular control by α- and γ-melanocyte-stimulating hormones. *Journal of Neuroscience* **16**, 5182–5188 (1996).

38. Mastrianni, J. A., Palkovits, M. & Kunos, G. Activation of brainstem endorphinergic neurons causes cardiovascular depression and facilitates baroreflex bradycardia. *Neuroscience* **33**, 559–566 (1989).

39. Lovelace, J. W., Ma, J. & Augustine, V. ll Defining cardioception : Heart-brain crosstalk. *Neuron* 1–4 (2024) doi:10.1016/j.neuron.2024.10.009.

40. Shivkumar, K. *et al.* Clinical neurocardiology defining the value of neuroscience-based cardiovascular therapeutics. *Journal of Physiology* **594**, 3911–3954 (2016).

41. Klein, A. S., Dolensek, N., Weiand, C. & Gogolla, N. Fear balance is maintained by bodily feedback to the insular cortex in mice. *Science (1979).* **374**, 1010–1015 (2021).

42. Hsueh, B. *et al.* Cardiogenic control of affective behavioural state. *Nature* https://doi.org/10.1038/s41586-023-05748-8 (2023) doi:10.1038/s41586-023-05748-8.

828 43. Yao, Y. *et al.* Cardiovascular baroreflex circuit moonlights in sleep control.
829 *Neuron* **0**, (2022).

830 44. Han, Z., Yi, P., Li, X. & Olson, E. N. Hand, an evolutionarily conserved bHLH
831 transcription factor required for Drosophila cardiogenesis and hematopoiesis.
832 *Development* **133**, 1175–1182 (2006).

833 45. Han, Z. & Olson, E. N. Hand is a direct target of Tinman and GATA factors
834 during Drosophila cardiogenesis and hematopoiesis. *Development* **132**, 3525–
835 3536 (2005).

836 46. Sellin, J., Albrecht, S., Kölsch, V. & Paululat, A. Dynamics of heart
837 differentiation, visualized utilizing heart enhancer elements of the Drosophila
838 melanogaster bHLH transcription factor Hand. *Gene Expression Patterns* **6**, 360–
839 375 (2006).

840 47. Wessells, R. J. & Bodmer, R. Screening assays for heart function mutants in
841 Drosophila. *Biotechniques* **37**, 58–66 (2004).

842 48. Hillyer, J. F. & Pass, G. The Insect Circulatory System: Structure, Function, and
843 Evolution. https://doi.org/10.1146/annurev-ento-011019 (2019)
844 doi:10.1146/annurev-ento-011019.

845 49. Rotstein, B. & Paululat, A. On the morphology of the drosophila heart. *Journal*
846 *of Cardiovascular Development and Disease* vol. 3 Preprint at
847 https://doi.org/10.3390/jcdd3020015 (2016).

848 50. Dulcis, D. & Levine, R. B. Glutamatergic innervation of the heart initiates
849 retrograde contractions in adult Drosophila melanogaster. *Journal of*
850 *Neuroscience* **25**, 271–280 (2005).

851 51. Dulcis, D. & Levine, R. B. Innervation of the heart of the adult fruit fly,
852 Drosophila melanogaster. *Journal of Comparative Neurology* **465**, 560–578
853 (2003).

854 52. Barrios, N., Farias, M. & Moita, M. A. Threat induces cardiac and metabolic
855 changes that negatively impact survival in flies. *Current Biology* **0**, (2021).

856 53. Tsuji, M., Nishizuka, Y. & Emoto, K. Threat gates visual aversion via theta
857 activity in Tachykinergic neurons. *Nat. Commun.* **14**, 3987 (2023).

858 54. Pereira, T. D. *et al.* SLEAP: A deep learning system for multi-animal pose
859 tracking. *Nature Methods 2022 19:4* **19**, 486–495 (2022).

860 55. Tsubouchi, A. *et al.* Topological and modality - specific representation of
861 somatosensory information in the fly brain. *Science* **623**, 615–623 (2017).

862 56. Zhang, N., Guo, L. & Simpson, J. H. Spatial Comparisons of Mechanosensory
863 Information Govern the Grooming Sequence in Drosophila. *Current Biology* **30**,
864 988-1001.e4 (2020).

865 57. Lebestky, T. *et al.* Two Different Forms of Arousal in Drosophila Are Oppositely
866 Regulated by the Dopamine D1 Receptor Ortholog DopR via Distinct Neural
867 Circuits. *Neuron* **64**, 522–536 (2009).

868 58. Zhang, F., Zhao, Y. & Han, Z. An in vivo functional analysis system for renal
869 gene discovery in Drosophila pericardial nephrocytes. *Journal of the American*
870 *Society of Nephrology* **24**, 191–197 (2013).

871 59. Keller, N. R. *et al.* Norepinephrine transporter-deficient mice exhibit excessive
872 tachycardia and elevated blood pressure with wakefulness and activity.
873 *Circulation* **110**, 1191–1196 (2004).

874 60. Zornik, E., Paisley, K. & Nichols, R. Neural transmitters and a peptide modulate
875 Drosophila heart rate. *Peptides (N.Y.).* **20**, 45–51 (1999).

876 61. Zhu, Y. C., Yocom, E., Sifers, J., Uradu, H. & Cooper, R. L. Modulatory effects
877 on Drosophila larva hearts: room temperature, acute and chronic cold stress. *J.*
878 *Comp. Physiol. B* **186**, 829–41 (2016).

879 62. Johnson, E., Ringo, J. & Dowse, H. Modulation of drosophila heartbeat by
880 neurotransmitters. *J. Comp. Physiol. B* **167**, 89–97 (1997).

881 63. Hillyer, J. F. Insect heart rhythmicity is modulated by evolutionarily conserved
882 neuropeptides and neurotransmitters. *Current Opinion in Insect Science* vol. 29
883 41–48 Preprint at https://doi.org/10.1016/j.cois.2018.06.002 (2018).

884 64. Majeed, Z. R., Stacy, A. & Cooper, R. L. Pharmacological and genetic
885 identification of serotonin receptor subtypes on Drosophila larval heart and aorta.
886 *J. Comp. Physiol. B* **184**, 205–219 (2014).

887 65. Johnson, E., Sherry, T., Ringo, J. & Dowse, H. Modulation of the cardiac
888 pacemaker of Drosophila: Cellular mechanisms. *J. Comp. Physiol. B* **172**, 227–
889 236 (2002).

890 66. Schroeder, C. & Jordan, J. Norepinephrine transporter function and human
891 cardiovascular disease. *American Journal of Physiology - Heart and Circulatory*
892 *Physiology* vol. 303 1273–1282 Preprint at
893 https://doi.org/10.1152/ajpheart.00492.2012 (2012).

894 67. Sujkowski, A., Gretzinger, A., Soave, N., Todi, S. V. & Wessells, R. Alpha- and
895 beta-adrenergic octopamine receptors in muscle and heart are required for
896 Drosophila exercise adaptations. *PLoS Genet.* **16**, e1008778 (2020).

897 68. Schiemann, R. *et al.* Identification and In Vivo Characterisation of Cardioactive
898 Peptides in Drosophila melanogaster. *Int. J. Mol. Sci.* **20**, 2 (2018).

899 69. Xie, T. *et al.* A Genetic Toolkit for Dissecting Dopamine Circuit Function in
900 Drosophila. *Cell Rep.* **23**, 652 (2018).

901 70. Mao, Z. & Davis, R. L. Eight different types of dopaminergic neurons innervate
902 the Drosophila mushroom body neuropil: Anatomical and physiological
903 heterogeneity. *Front. Neural Circuits* **3**, 612 (2009).

904 71. Luan, H., Peabody, N. C., Vinson, C. R. R. & White, B. H. Refined Spatial
905 Manipulation of Neuronal Function by Combinatorial Restriction of Transgene
906 Expression. *Neuron* **52**, 425–436 (2006).

907 72. Clements, J. *et al.* NeuronBridge: an intuitive web application for neuronal
908 morphology search across large data sets. *BMC Bioinformatics* **25**, 1–25 (2024).

909 73. Mais, L. *et al.* PatchPerPixMatch for Automated 3d Search of Neuronal
910 Morphologies in Light Microscopy. *bioRxiv* 2021.07.23.453511 (2021).

911 74. Wu, G. *et al.* Opposing GPCR signaling programs protein intake setpoint in
912 Drosophila. *Cell* https://doi.org/10.1016/j.cell.2024.07.047 (2024)
913 doi:10.1016/j.cell.2024.07.047.

914 75. Liu, Q. *et al.* Branch-specific plasticity of a bifunctional dopamine circuit
915 encodes protein hunger. *Science* **356**, 534–539 (2017).

916 76. Dana, H. *et al.* High-performance calcium sensors for imaging activity in
917 neuronal populations and microcompartments. *Nat. Methods* **16**, 649–657 (2019).

918 77. Men, J. *et al.* Non-invasive red-light optogenetic control of Drosophila cardiac
919 function. *Commun. Biol.* **3**, 336 (2020).

920 78. Skora, L. I., Livermore, J. J. A. & Roelofs, K. The functional role of cardiac
921 activity in perception and action. *Neurosci. Biobehav. Rev.* **137**, 104655 (2022).

922 79. Koba, S., Inoue, R. & Watanabe, T. Role played by periaqueductal gray neurons
923 in parasympathetically mediated fear bradycardia in conscious rats. *Physiol. Rep.*
924 **4**, e12831 (2016).

925 80. Barrios, N., Farias, M. & Moita, M. A. Threat induces cardiac and metabolic
926 changes that negatively impact survival in flies. *Current Biology* **0**, (2021).

927 81. Neumann, J., Hofmann, B., Dhein, S. & Gergs, U. Role of Dopamine in the Heart
928 in Health and Disease. *International Journal of Molecular Sciences 2023, Vol.*
929 *24, Page 5042* **24**, 5042 (2023).

930 82. Ziegler, M. G., Kennedy, B., Holland, O. B., Murphy, D. & Lake, C. R. The
931 effects of dopamine agonists on human cardiovascular and sympathetic nervous
932 systems. *Int. J. Clin. Pharmacol.* **23**, 175–9 (1985).

933 83. Kirouac, G. J. & Pittman, Q. J. A projection from the ventral tegmental area to
934 the periaqueductal gray involved in cardiovascular regulation. *Am. J. Physiol.*
935 *Regul. Integr. Comp. Physiol.* **278**, R1643-50 (2000).

936 84. Sato, Y., Matsumoto, M. & Koganezawa, T. The dopaminergic system mediates
937 the lateral habenula-induced autonomic cardiovascular responses. *Front. Physiol.*
938 **15**, 1496726 (2024).

939 85. Van Vactor, D. L., Cagan, R. L., Krämer, H. & Zipursky, S. L. Induction in the
940 developing compound eye of Drosophila: Multiple mechanisms restrict R7
941 induction to a single retinal precursor cell. *Cell* **67**, 1145–1155 (1991).

942 86. Hummel, T. & Zipursky, S. L. Afferent induction of olfactory glomeruli requires
943 N-cadherin. *Neuron* **42**, 77–88 (2004).

944

945

946 **TABLES**

947 **Supplementary Data 1 List of genotypes and sample sizes used in this study**

948 **Supplementary Data 2 Statistics of data presented in this study**

949

950 **MOVIES**

951 **Supplementary Movie 1** An air puff induces cardiac deceleration and promotes
952 locomotion. A 50 mL/min puff is applied in the middle of the movie, as indicated by the
953 red text that appears on the top left panel of the movie. The bottom left panel shows a
954 behavioral recording, with automated body parts tracking (blue dots and lines)
955 superimposed on the raw data. The top right panel shows the raw heartbeat recording,
956 and the bottom right panel shows the pixel-wise, color-coded optical flow (color-to-
957 direction mapping is shown on the top right of the panel). The playback speed is
958 reduced to 0.25 of the original file.
959

960 **Supplementary Movie 2** A train of 10 air puffs induce cardiac deceleration in a
961 Hand>GFP fly. The playback speed is reduced to 0.25 of the original file.
962

963 **Supplementary Movie 3** Air puffs activate DA-WED neurons. The left panel shows a
964 schematic of the DA-WED neurons and the actual calcium imaging data (averaged
965 over the total recording), capturing both DA-WED neurons in the right hemisphere.
966 An arrow indicates the neuron shown on the right panel. The right panel shows
967 GCaMP signals at time 0 on the top, and the time-lapse imaging from there during
968 which air puffs were applied.
969

970 **Supplementary Movie 4** Optogenetic activation of DA-WED neurons induces cardiac
971 deceleration and promotes locomotion. The playback speed is reduced to 0.25 of the
972 original file.
973

974 **Supplementary Movie 5** Optogenetic cardiac deceleration promotes locomotion. The
975 playback speed is reduced to 0.25 of the original file.

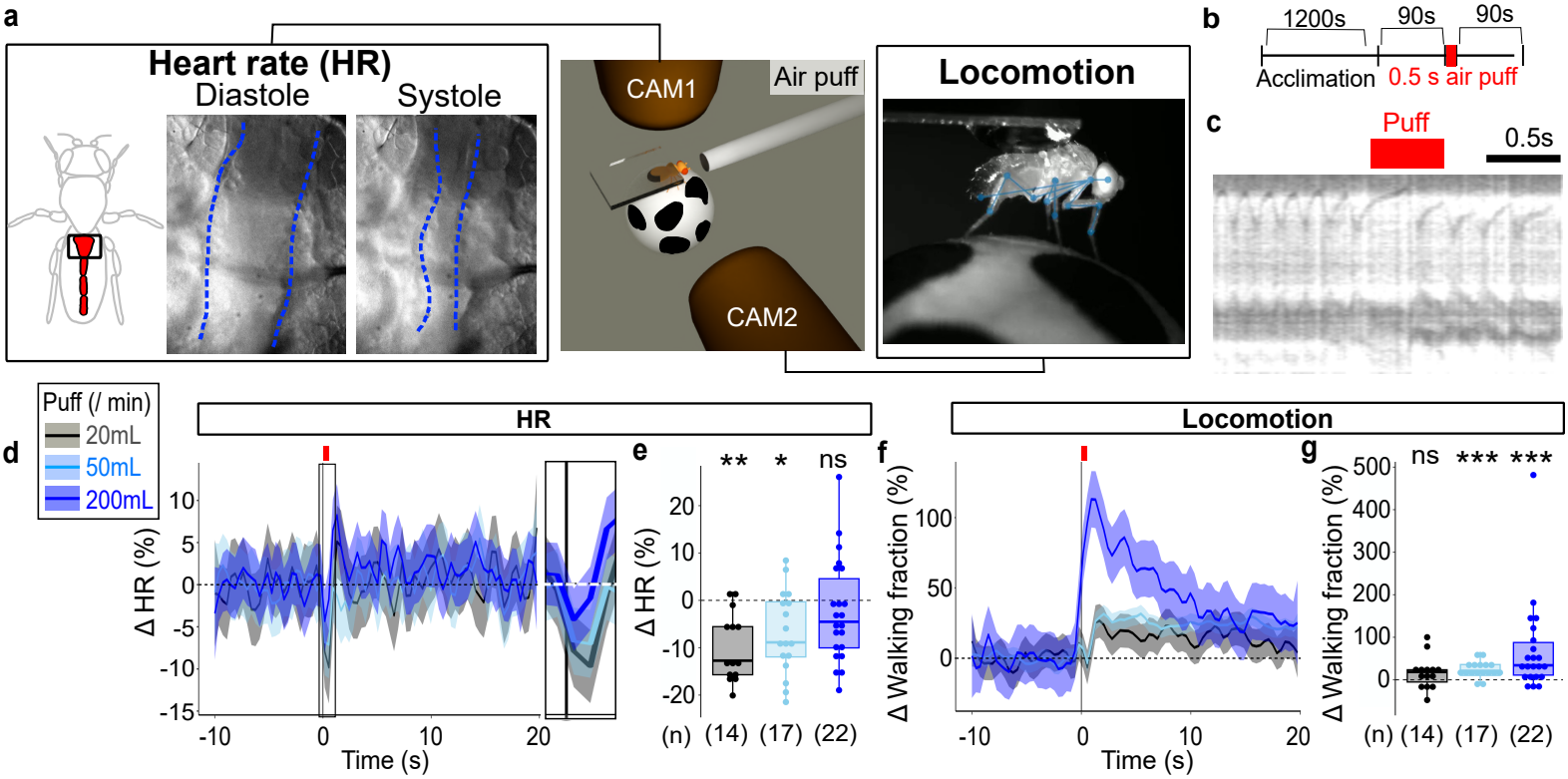

Fig. 1 Mechanical threat induces cardiac deceleration and locomotion

a. Schematics of the paradigm. The fly is fixed on an air-supported ball. Left: the heart rate (HR) was videotaped by an IR-sensitive camera from the dorsal side through the cuticle ("CAM1"). Of the four cardiac chambers, our system videotaped the chamber closest to the thorax called conical chamber. We could easily distinguish diastole and systole in the captured video (blue dashed lines indicate the heart wall). Right: simultaneously, locomotion was videotaped from the right side of the fly ("CAM2"). Blue dots and lines indicate automatically tracked body parts. **b.** The time course of the experiment. An air puffs of 0.5 s was applied once. The trial was repeated 10 times for each fly, the results of which were averaged. **c.** An example M-mode of the heartbeat. An air puff was applied during the red-shaded time window. **d.** Time course of the HR (% change from baseline defined as the average during the 10 s preceding puff onset). N = 14, 17, 22 for 20mL/min (gray), 50mL/min (sky blue), and 200mL/min (dark blue), respectively. The inlet shows the magnified view of the cardiac deceleration indicated by the box. **e.** Change in HR, calculated for each fly as the % difference between the mean fraction during the 1 s following stimulation onset and the mean fraction during the 10 s baseline period preceding stimulation. N = 14, 17, 22 for 20mL/min (gray), 50mL/min (sky blue), and 200mL/min (dark blue), respectively. **$p < 0.01$, *$p < 0.05$, n.s.: $p > 0.05$, Wilcoxon's signed rank test followed by Bonfferoni correction. **f.** Time course of the walking fraction (% change from baseline defined as the mean fraction during the 10 s preceding puff onset). N = 14, 17, 22 for 20mL/min (gray), 50mL/min (sky blue), and 200mL/min (dark blue), respectively. ***$p < 0.001$, n.s.: $p > 0.05$, Wilcoxon's signed rank test followed by Bonfferoni correction. **g.** Change in walking fraction, calculated for each fly as the % difference between the mean fraction during the 10 s following stimulation onset and the mean fraction during the 10 s baseline period preceding stimulation. N = 14, 17, 22 for 20mL/min (gray), 50mL/min (sky blue), and 200mL/min (dark blue), respectively. ***$p < 0.001$, n.s.: $p > 0.05$, Wilcoxon's signed rank test followed by Bonfferoni correction.

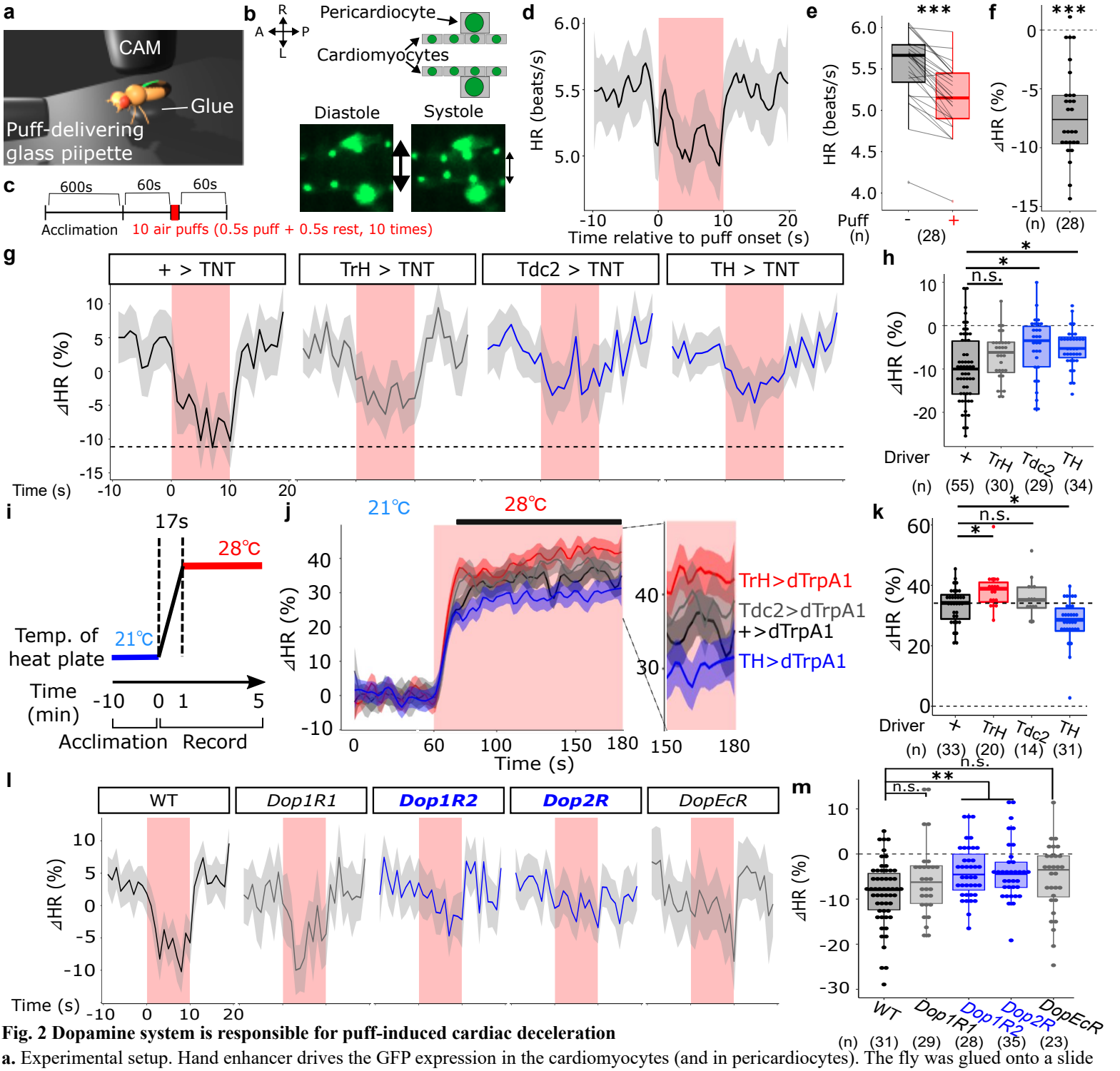

Fig. 2 Dopamine system is responsible for puff-induced cardiac deceleration

a. Experimental setup. Hand enhancer drives the GFP expression in the cardiomyocytes (and in pericardiocytes). The fly was glued onto a slide glass, and the GFP signals were acquired through the intact cuticle. The air puffs were applied frontally to the fly's head. **b.** Example heartbeat. (Upper) Cartoon of the acquired image. Two rows of small cardiomyocytes and one pair of large pericardiocytes are visible. (Lower) Diastole and systole can be distinguished by the changing distance between two rows of cardiomyocytes (arrows). **c.** The time course of the experiment. Air puffs of 0.5 s were applied at 1 Hz for 10 times (totalling 10 s). The trial was repeated twice for each fly, the results of which were averaged. **d.** Time course of the HR. Air puffs are applied during red-shaded window. Lines and shaded areas represent means and SEM, respectively. N = 28. **e.** The HR averaged during puff application window ("puff +") vs 10 s before puff application ("puff -"). Each line corresponds to each fly. N = 28, ***$p < 0.001$, two-tailed *t*-test. **f.** Difference between puff+ HR and puff- HR, calculated for each fly. N = 28, ***$p < 0.001$, two-tailed *t*-test. **g.** Time course of the HR (% change from baseline defined as the average during the 10 s preceding puff onset). Air puffs were applied during the red-shaded time window. Lines and shaded areas represent means and SEM, respectively. TNT expression is driven by indicated drivers. "+" indicates driver-less control. Dashed line shows the lowest mean of "+" control during puffs. N = 55, 30, 29, 34, for +, TrH, Tdc2, TH, respectively. **h.** Change in HR, calculated for each fly as the % difference between the mean HR during the 10 s stimulation period and the mean HR during the 10 s baseline period preceding stimulation. N = 55, 30, 29, 34, for +, TrH, Tdc2, TH, respectively. *$p < 0.05$, n.s.: $p > 0.05$, Dunn's test. **i.** Time course of the experiment. The heat plate beneath the slide glass warmed up the fly. The temperature of the slide glass is held at 21°C for 10 min and ramped up to 28°C for 5min. Note it took approximately 17 s for the temperature to ramp from 21°C to 28°C. **j.** Time course of the HR, shown as % change from average HR at 21°C. Temperature was rampted from 21°C to 28°C during red-shaded window. **k.** % Changes in the HR (28°C vs 21°C) from the baseline (average over initial 60 s) averaged over 75s - 180s window (shown as black bar in j.). N = 33, 20, 14, 31, for +, TrH, Tdc2, TH, respectively. *$p < 0.05$, n.s.: $p > 0.05$, Dunn's test. The upper dashed line shows the median of "+" control. **l.** Time course of the HR (% change from baseline defined as the average during the 10 s preceding puff onset). Air puffs were applied during the red-shaded time window. Lines and shaded areas represent means and SEM, respectively. N = 31, 29, 28, 35, 23, for +, WT, *Dop1R1*, *Dop1R2*, *Dop2R*, *DopEcR*, respectively. **m.** Change in HR, calculated for each fly as the % difference between the mean HR during the 10 s stimulation period and the HR HR during the 10 s baseline period preceding stimulation. N = 31, 29, 28, 35, 23, for +, WT, *Dop1R1*, *Dop1R2*, *Dop2R*, *DopEcR*, respectively. **$p < 0.01$, n.s.: $p > 0.05$, Dunn's test.

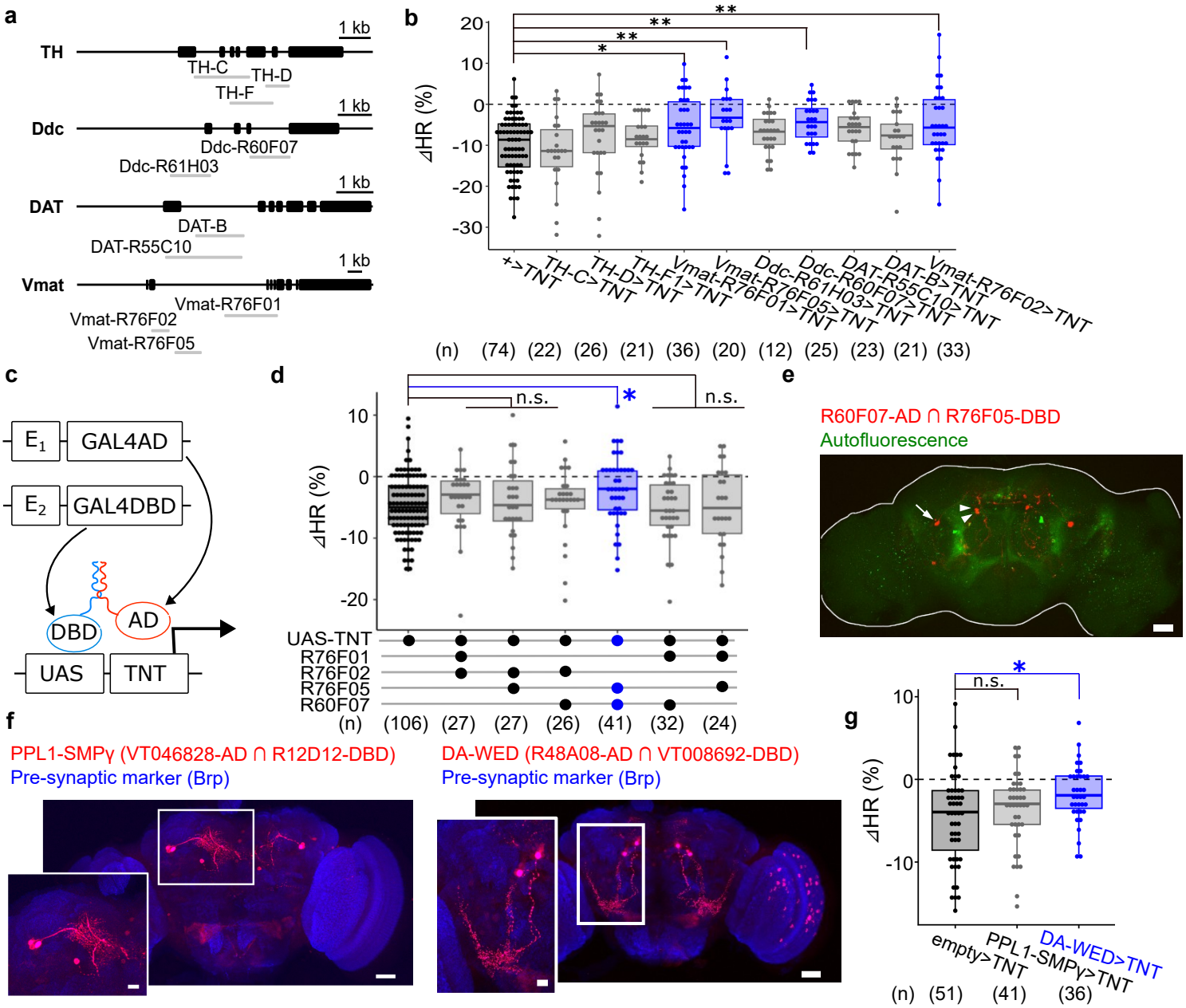

Fig. 3 Two pairs of dopaminergic neurons in the brain are paritally indispensable for cardiac deceleration

a. AsSchematic of different DA-related GAL4 drivers. **b.** Change in HR, calculated for each fly as the % difference between the mean HR during the 10 s stimulation period and the HR HR during the 10 s baseline period preceding stimulation. N = 74, 22, 26, 21, 36, 20, 12, 25, 23, for +, TH-C, TH-D, TH-F1, Vmat-R76F01, Vmat-R76F05, Ddc-R61H03, Ddc-R60F07, DAT-R55C10, respectively. **p < 0.01, *p < 0.05, n.s. (data shown in gray): p > 0.05, Dunnett's test. **c.** A schematic of split-GAL4 strategy. **d.** Change in HR, calculated for each fly as the % difference between the mean HR during the 10 s stimulation period and the HR HR during the 10 s baseline period preceding stimulation. N = 106, 27, 27, 26, 41, 32, 24, for driver-less control, R76F01 ∩ R76F02, R76F02 ∩ R76F05, R76F01 ∩ R76F02, R76F02 ∩ R76F07, R76F05 ∩ R60F07, R76F01 ∩ R60F07, R76F01 ∩ R76F05, respectively. *p < 0.05, n.s.: p > 0.05, Dunn's test. **e.** Brain of R60F07-AD ∩ R76F01-DBD>mCherry (red). An arrow indicates the soma of PPL1-SMPγ, while arrowheads indicate the soma of DA-WED. Scale bar: 25 um. Similar results were obtained across 3 independent samples. **f.** Brains of VT046828-AD ∩ R12D12-DBD>mCherry and R48A08-AD ∩ VT008692-DBD>mCherry (red) immunostained with anti-neuropil marker nc82 (blue). Scale bars: 25 um (inlet: 5 um). Similar results were obtained across 5 independent samples for each genotype. **g.** Change in HR, calculated for each fly as the % difference between the mean HR during the 10 s stimulation period and the HR HR during the 10 s baseline period preceding stimulation. N = 51, 41, 36 for empty>TNT, PPL1-SMPγ>TNT, DA-WED>TNT, respectively. *p < 0.05, n.s.: p > 0.05, Dunnett's test.

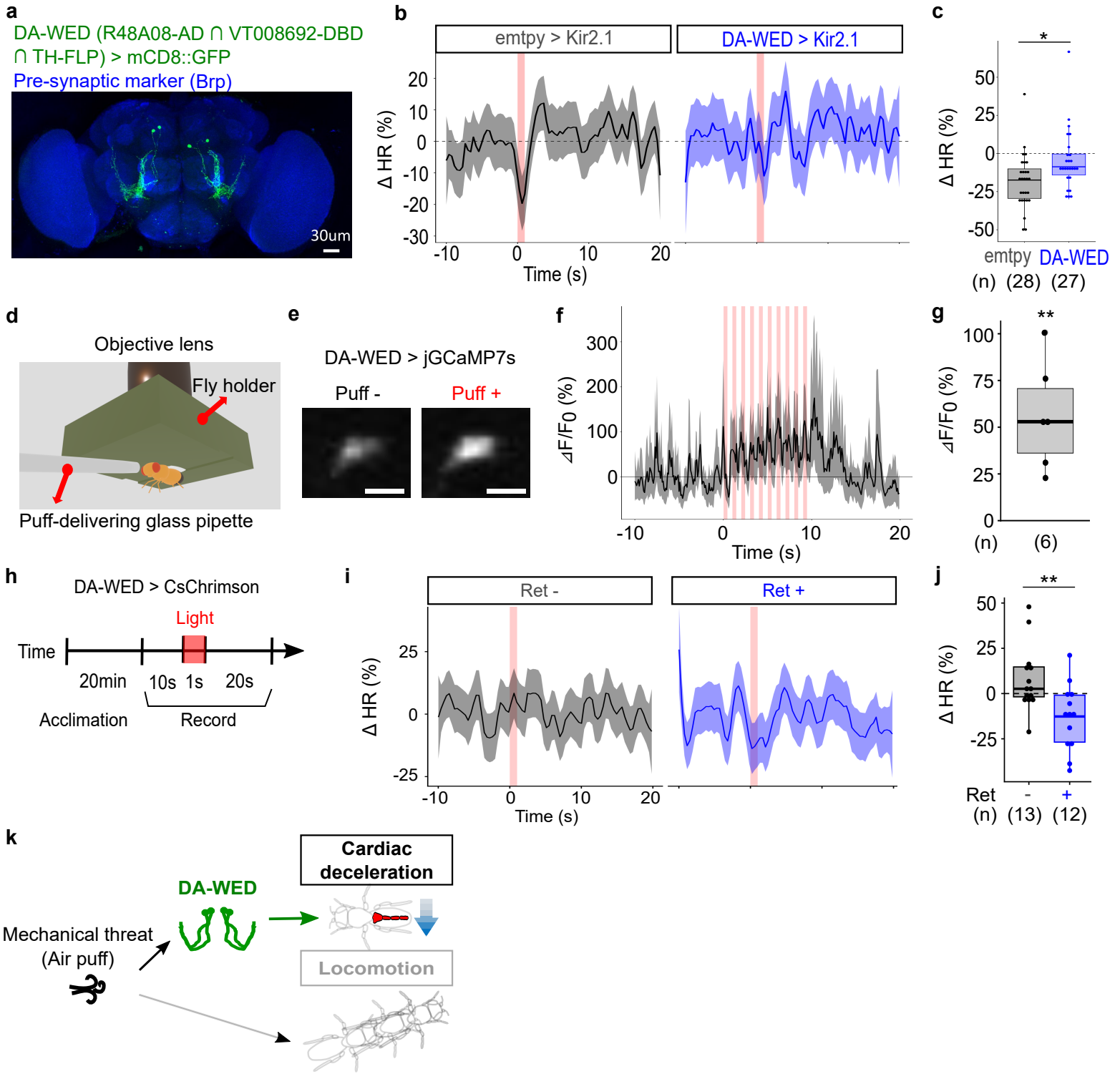

Fig. 4 DA-WED neurons are responsible for puff-induced cardiac deceleration

a. The brain of R48A08-AD ∩ VT008692-DBD ∩ TH-FLP>mCD8::GFP (green) immunostained with anti-neuropil marker nc82 (blue). Scale bar: 30 um. Similar results were obtained across 5 independent samples. **b.** Time course of the HR (% change from baseline defined as the average during the 10 s preceding puff onset). Air puff was applied during the red-shaded time window. Lines and shaded areas represent means and SEM, respectively. N = 28, 27, for empty>Kir2.1, DA-WED>Kir2.1, respectively. **c.** Change in HR, calculated for each fly as the % difference between the mean HR during the 1 s following stimulation onset and the mean HR during the 10 s baseline period preceding stimulation. N = 28, 27, for empty>Kir2.1, DA-WED>Kir2.1, respectively. *p < 0.05, Two-tailed *t*-test. **d.** Experimental setup. **e.** Representative images of DA-WED neurons expressing GCaMP7s before and during puff application. Scale bar: 5μm. **f.** Time course of $\Delta F/F_0$. Puffs were applied at 1Hz for 10 times (over 10 s), as indicated by red-shaded boxes. N = 6 flies. **g.** $\Delta F/F_0$ averaged over 10s of puff application. When multiple neurons were recorded from the same fly (max 4 neurons per fly), results were averaged so that each dot represents one fly. N = 6 flies. two-tailed *t*-test. **p < 0.01. **h.** Time course of the experiment. After 20 min of acclimation, the heartbeat of the fly expressing light-gated cation channel CsChrimson in DA-WED neurons, with ("Ret +") or without ("Ret -") being fed with the co-factor all-trans retinal (ATR) for 2 days prior to experiment, was recorded for 10s, followed by 1s of light application, and 20s of recording. **i.** Time course of the HR (% change from baseline defined as the average during the 10 s preceding puff onset). Red light was shined during the red-shaded time window. Lines and shaded areas represent means and SEM, respectively. N = 19, 22, for Ret-, Ret+, respectively. **j.** Change in HR, calculated for each fly as the % difference between the mean HR during the 1 s following stimulation onset and the mean HR during the 10 s baseline period preceding stimulation. N = 13, 12, for Ret-, Ret+, respectively. *p < 0.05, two-tailed *t*-test. **k.** Model.

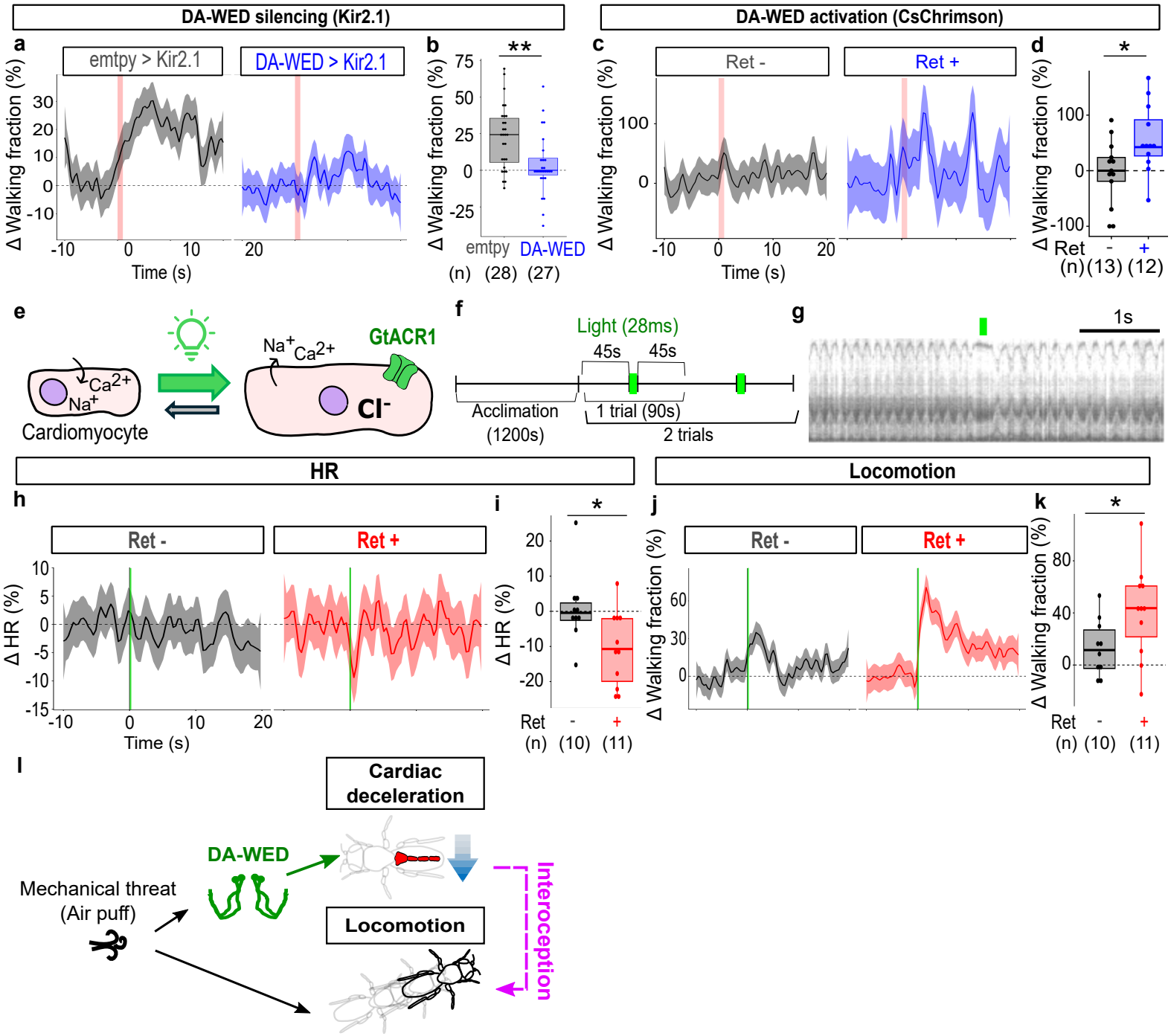

Fig. 5 Cardiac interoception possibly contributes to threat-induced locomotion

a. Time course of the walking fraction (% change from baseline defined as the mean fraction during the 10 s preceding puff onset). An air puff was applied during the red-shaded time window. Lines and shaded areas represent means and SEM, respectively. N = 28, 27, for empty>Kir2.1, DA-WED>Kir2.1, respectively. **b.** Change in walking fraction, calculated for each fly as the % difference between the mean fraction during the 10 s following stimulation onset and the mean fraction during the 10 s baseline period preceding stimulation. N = 28, 27, for empty>Kir2.1, DA-WED>Kir2.1, respectively. **p < 0.01, Two-tailed *t*-test. **c.** Time course of the walking fraction (% change from baseline defined as the mean fraction during the 10 s preceding puff onset). Red light was applied during the red-shaded time window. Lines and shaded areas represent means and SEM, respectively. N = 13, 12, for ret -, +, respectively. **d.** Change in walking fraction, calculated for each fly as the % difference between the mean fraction during the 10 s following stimulation onset and the mean fraction during the 10 s baseline period preceding stimulation. N = 13, 12, for ret -, +, respectively. **p < 0.01, Two-tailed *t*-test. **e.** A schematic of the strategy. Cardiomyocytes beat by oscillating between shrunk (systole) and relaxed (diastole) states. Diastole is driven by efflux of cation and resultant hyperpolarization. We expressed a light-gated anion channel GtACR1 in cardiomyocytes using Hand-GAL4, thus artificially driving hyperpolarization by shining light. **f.** Time course of the experiment. After 20 min of acclimation, the heartbeat of the fly expressing GtACR1 in cardiomyocytes, with or without being fed with the co-factor all-trans retinal (ATR) for 2 days prior to experiment, was recorded for 90s, followed by a 28ms light pulse, and 45s of recording. The experiment was repeated twice for each fly. **g.** An example M-mode during optogenetic cardiac deceleration. Green bar indicates when the light was shined. **h.** Time course of the HR (% change from baseline defined as the average during the 10 s preceding puff onset). Green light was shined during the breen-shaded time window. Lines and shaded areas represent means and SEM, respectively. N = 10, 11, for ret -, ret +, respectively. **i.** Change in HR, calculated for each fly as the % difference between the mean HR during the 1 s following stimulation onset and the mean HR during the 10 s baseline period preceding stimulation. N = 10, 11, for ret -, ret +, respectively. *p < 0.05, Two-tailed *t*-test. **j.** Time course of the walking fraction (% change from baseline defined as the mean fraction during the 10 s preceding puff onset). Light was shined during the green-shaded time window. Lines and shaded areas represent means and SEM, respectively. N = 10, 11, for ret -, ret +, respectively. **k.** Change in walking fraction, calculated for each fly as the % difference between the mean fraction during the 10 s following stimulation onset and the mean fraction during the 10 s baseline period preceding stimulation. N = 10, 11, for ret -, ret +, respectively. *p < 0.05, two-tailed *t*-test. **l.** Model.